Apoptosis (2012) 17:1170–1181
DOI 10.1007/s10495-012-0760-z

ORIGINAL PAPER

2,3,7,8-Tetrachlorodibenzo-*p*-dioxin induces apoptosis by disruption of intracellular calcium homeostasis in human neuronal cell line SHSY5Y

Antonio Morales-Hernández · Francisco J. Sánchez-Martín · María P. Hortigón-Vinagre · Fernando Henao · Jaime M. Merino

Published online: 18 September 2012

Abstract The persistent xenobiotic agent 2,3,7,8-tetrachlorodibenzo-*p*-dioxin (TCDD) induces neurotoxic effects that alters neurodevelopment and behavior both during development and adulthood. There are many ongoing efforts to determine the molecular mechanisms of TCDD-mediated neurotoxicity, the signaling pathways involved and its molecular targets in neurons. In this work, we have used SHSY5Y human neuroblastoma cells to characterize the TCDD-induced toxicity. TCDD produces a loss of viability linked to an increased caspase-3 activity, PARP-1 fragmentation, DNA laddering, nuclear fragmentation and hypodiploid (apoptotic) DNA content, in a similar way than staurosporine, a prototypical molecule of apoptosis induction. In addition, TCDD produces a decrease of mitochondrial membrane potential and an increase of intracellular calcium concentration ($P < 0.05$). Finally, based on the high lipophilic properties of the dioxin, we test the TCDD effect on the membrane integrity using sarcoplasmic reticulum vesicles as a model. TCDD produces calcium efflux through the membrane and an anisotropy decrease ($P < 0.05$) that reflects an increase in membrane fluidity. Altogether these results support the hypothesis that TCDD toxicity in SHSY5Y neuroblastoma cells provokes the disruption of calcium homeostasis, probably affecting membrane structural integrity, leading to an apoptotic process.

Keywords TCDD · Apoptosis · Calcium · Human neuronal cell line SHSY5Y · Neurotoxicity

Introduction

Dioxins are currently a very relevant environmental contaminant group of molecules that can be included to polycyclic aromatics hydrocarbons (PAHs) [1]. These toxins are produced as by-products of several industrial processes (i.e. manufacture of chemicals and pesticides, bleaching of paper pulp, etc.) and combustion activities (i.e. municipal solid waste incineration, burning woods, etc.) [2, 3]. The prototypical dioxin 2,3,7,8-tetrachlorodibenzo-*p*-dioxin (TCDD) is a persistent xenobiotic agent which can produce toxicity and cancer [4]. Due to the fact that TCDD binds with high affinity to the aryl hydrocarbon receptor (AhR) it is assumed that its toxic and carcinogenic effects are mainly mediated by this receptor [5]. However, there are many aspects of the TCDD toxicity that are misunderstood and, consequently, still to be defined. Thus, the studies directed to elucidate the molecular mechanisms implicated in this toxicity are of great relevance. Besides, neurotoxic effects of dioxin are less deeply analyzed in comparison with its carcinogenic action. In vivo studies in rhesus monkey showed that TCDD-induced changes in behavior [6] and long term cognitive deficits [7], both during development and in adulthood. More significant studies were done in humans after gestational exposure to TCDD and displayed important alterations in neurodevelopment [8–11]. Moreover, TCDD alters normal rat brain development and produces cognitive disability and motor dysfunction [12, 13] and abnormal cerebellar maturation in both humans and rodents

Electronic supplementary material The online version of this article (doi:10.1007/s10495-012-0760-z) contains supplementary material, which is available to authorized users.

A. Morales-Hernández · F. J. Sánchez-Martín · M. P. Hortigón-Vinagre · F. Henao · J. M. Merino (✉)
Departamento de Bioquímica y Biología Molecular, Facultad de Ciencias, Universidad de Extremadura, 06071 Badajoz, Spain
e-mail: jmmerino@unex.es

[14]. Data from human studies and experimental observations provide firm evidences that PCBs and dioxins negatively affect thyroid function and PCBs have been suggested to interfere with neural development through thyroid function modulation [15]. But again, the molecular mechanisms underlying TCDD neurotoxicity are poorly understood.

There are several in vitro studies, using cerebellar granule cells and cortical neurons, performed to determine the mechanisms by which TCDD causes its neurotoxicity. These works mainly linked TCDD toxicity with an increase in the intracellular calcium concentration and, as a consequence, neuronal death takes place due to a massive generation of reactive oxygen species (ROS) [16–18]. The mechanisms by which TCDD could induce the increase in calcium concentration are unknown. Therefore it is of high interest to further study TCDD neurotoxicity to determine the signaling pathways and to identify the molecular targets of the dioxin.

TCDD is a molecule with high lipophilic properties [19]. Due to this, it may be suggested that, at least in part, its toxic effects could be due to a disruption of calcium homeostasis as a consequence of alterations in cell membrane integrity. Also, there are evidences that other environmental contaminants (i.e. perfluorinated compounds) or products of lipid peroxidation (i.e. 4-hydroxy-2-nonenal) can alter calcium homeostasis through alterations in cell membrane properties [20, 21]. Maintenance of calcium homeostasis in the cell is very important because this ion is involved in neuronal plasticity, learning and memory and neuronal survival [22].

SHSY5Y cells are a subline of human SK-N-SH cell line and they have many biochemical and functional characteristic of neurons [23]. While primary cultures undergo survival and degeneration problems, as well as the appearance of genetic abnormalities such as trisomies, these stable cell lines avoid these problems [24]. Also, SHSY5Y cells responses are similar to those found in human primary culture to cytotoxic compounds [25]. Thus, this cell line represents a useful model to be used in neurotoxic research.

The effects of TCDD and related substances on apoptosis signaling are a matter of discussion, with both inducing and repressing effects, as reviewed in [26]. Previous studies from our laboratory have described the toxic effects of TCDD on NGF-differentiated PC12 cells [27] and cerebellar granule cells from mouse [28]. The results indicate that TCDD induces cell death through an apoptotic process AhR-dependent, albeit on NGF-differentiated PC12 cells the role of AhR was not prominent. In this paper, we study TCDD effects in SHSY5Y cells aiming to determine the mechanisms by which this dioxin induces neurotoxicity.

Materials and methods

SHSY5Y cells cultures

Human neuroblastoma (SHSY5Y) cells were grown in complete medium containing Dulbecco's modified Eagle's medium (DMEM, Hyclone) with the F-12 nutrients mixture, supplemented with 10 % (v/v) fetal bovine serum (Sigma), 2 mM L-glutamine (Gibco) and 1 % (v/v) antibiotic/antimycotic mixture (Gibco). Cultures were maintained at 37 °C in a humidified atmosphere containing 5 % CO_2 until reaching the desired confluence. All the experiments were performed at 80–85 % confluence.

TCDD toxicity assays

To determine the TCDD toxicity, SHSY5Y cells were cultured in 24-well plates. The cells were exposed for 90 min to different TCDD concentrations (ranging from 10–1,000 nM) at 37 °C in the culture medium. The toxic insult was terminated by the removal of the medium, followed by the addition of fresh culture medium. When applicable, cultures were returned to the incubator (37 °C/5 % CO_2), and cell death was assessed 18–24 h postinsult using the 3-[4,5-dimethylthiazol-2-yl]-2,5-diphenyl-tetrazolium (MTT) reduction or the trypan blue exclusion assays as described below. The EC_{50} value for TCDD toxicity represents the 50 % of effect exerted by the dioxin in SHSY5Y cells and it was calculated using the logistic dose response curve from the Origin™ software.

Cell viability measurements by trypan blue exclusion and MTT reduction assays

Changes in cell viability were determined by MTT reduction assay as described by [29]. In brief, cultures were incubated at 37 °C for 1 h with basic saline solution (BSS, 137 mM NaCl, 3.5 mM KCl, 0.4 mM KH_2PO_4, 0.33 mM $Na_2HPO_4{\cdot}7H_2O$, 5 mM *N*-tris(hydroxymethyl)methyl-2-aminoethanesulfonic acid (TES) pH 7.4, 10 mM D-glucose) containing 150 μg/ml of MTT. The formazan generated by mitochondrial dehydrogenase activity of live cells were dissolved in dimethyl sulfoxide (Sigma) and quantified by measuring the difference in absorbance between 490 and 650 nm. Data are shown as percentage of control condition (100 %).

Alternatively, changes in cell viability were determined by using the trypan blue exclusion assay as previously described [30]. Cultures were incubated with trypan blue dye at 0.4 % (w/v) for 4 min, and then washed with BSS solution to eliminate the excess of the dye. Cells not stained were considered viable cells. Cells with blue stained nucleus were considered dead cells. The values

showed as cell death represent the percentage of non viable cells from total cells counted. A minimum of 500 cells were counted in 4–5 microscopic fields per plate. Three separate cultures and two plates per conditions were used, at least, for each experimental group. Data are shown as percentage of control condition (100 %).

Measurements of caspase-3 activity

Caspase 3 activity was measured as previously described [31]. The caspase 3 substrate used was *N*-Acetyl-Asp-Glu-Val-Asp-7-amido-4-methylcoumarin (Sigma). The fluorescence was measured with a spectrofluorimeter Cary Eclipse (Varian) using excitation and emission wavelengths of 360 and 460 nm. Data were calculated as fluorescence Units/μg protein. Data are presented as percentage relative to the activity measured in control cultures.

Nuclear morphology changes by DAPI labeling

SHSY5Y cells were cultured in 35 mm dishes. SHSY5Y cells were incubated with 250 nM TCDD for 90 min and up to 6 h of additional incubation without TCDD. Then, cells were incubated with 2 μM 4′,6-diamidino-2-phenylindole (DAPI) in PBS buffer (137 mM NaCl, 2.7 mM KCl, 1.47 mM KH_2PO_4 and 4.3 mM $Na_2HPO_4{\cdot}7H_2O$) for 5 min at 37 °C to evaluate nuclear morphology. After DAPI incubation cells were washed twice with PBS buffer. Fluorescence was visualized using fluorescence Axoplan Zeiss microscope with excitation and emission wavelengths of 350 and 460 nm, respectively.

DNA fragmentation analysis

DNA fragmentation was analyzed as described by [32]. Cell lysis was performed in 0.3 ml of a solution containing 5 mM Tris (pH 7.5), 20 mM EDTA and 0.5 % Triton X-100 for 1 h at 4 °C. Nuclei were precipitated by centrifugation at 10,000×*g* for 15 min. In order to obtain the DNA, supernatants were treated with 200 μg/ml proteinase K for 30 min at 60 °C and the DNA was purified by sequential extraction with phenol, phenol–chloroform (1:1) and chloroform and precipitated in ethanol-sodium acetate solution (overnight at −20 °C). Samples were then centrifuged for 30 min at 15,000×*g* at 4 °C, pellets were washed with 80 % ethanol and centrifuged again under the same conditions. Finally, DNA samples were resuspended in TE buffer or water and incubated with 30 μg/ml of RNase for 30 min at 37 °C. Samples were run in 1 % agarose gels and visualized by ethidium bromide staining and photographed.

Cell lysates and western immunoblot assay

SHSY5Y cells were washed with PBS and scraped from the plates with 1 ml of PBS at 4 °C. Then, samples were centrifuged at 14,000×*g* for 30 s and resuspended in 200 ml of lysis buffer containing 50 mM Tris–HCl pH 7.5, 2 mM EDTA, 2 mM EGTA, 270 mM sucrose, 10 mM b-glycerolphosphate, 5 mM sodium pyrophosphate, 50 mM sodium fluoride, 0.1 mM sodium orthovanadate, 0.1 % (v/v) *β*-mercaptoethanol and 4 mg/ml complete protease inhibitor cocktail (Roche). Cells suspensions were gently shaken for 15 min at 4 °C and centrifuged at 10,000×*g* for 10 min to obtain whole-cell extracts. Protein concentration was determined in the supernatants by the Coomassie protein assay system (Pierce) using bovine serum albumin as standard. For protein expression analysis by Western immunoblotting, 30 mg of protein were denatured, separated in sodium dodecyl sulphate (SDS)-8 % polyacrylamide gels and transferred to nitrocellulose membranes by electroblotting. Membranes were blocked for 2 h at room temperature in TBS-T (50 mM Tris–HCl pH 7.5, 150 mM NaCl, 0.2 % Tween-20) containing 5 % (w/v) nonfat milk. Blots were sequentially incubated with the primary anti-PARP-1 (Roche), anti-*β*-actin (Sigma) and secondary antibody HRP (Thermo Scientific), washed in TBS-T, and visualized using the SuperSignal luminol substrate (Pierce) and chemiluminescence analysis system ImageQuant 350 (General Electric). Molecular weights for poly(ADP-ribose) polymerase 1 (PARP-1) and *β*-actin bands are 113 and 42 kDa, respectively. Quantification of band intensity was evaluated using the ImageJ software.

Measurements of calcium concentration

For intracellular calcium concentration measurements SHSY5Y cells were cultured in 35 mm dishes. 15 min before the end of the different TCDD treatments the fluorescent dye Fluo 3-AM (Molecular Probes) was added at 2 μM to the culture medium and cells were incubated for 15 min at 37 °C. This incubation was performed in complete medium or in PBS for calcium or calcium-free assays, respectively. Samples were then washed twice with PBS buffer to eliminate the excess of dye. Fluorescence was visualized using fluorescence Axoplan Zeiss microscope with excitation and emission wavelengths of 505 and 527 nm, respectively. Fluorescence intensity was evaluated using the ImageJ software.

To measure the Ca^{2+} efflux in sarcoplasmic reticulum (SR) membranes (prepared as indicated below) in the presence of TCDD, the fluorescent dye Fura-2 pentapotassium salt (Invitrogen) was used. 10 mg/ml of SR membranes were loaded with Ca^{2+} in buffer containing 50 mM Tes-Tris pH 7.4, 100 mM KCl, 200 mM sucrose

and 2 mM Ca^{2+} for 90 min at 37 °C. Ca^{2+}-loaded SR membranes were diluted to 0.5 mg/ml in the same buffer without Ca^{2+}. The fluorescent probe Fura-2 at 5 μM concentration was added to measure the ratio of fluorescence at 340/380 excitation and 510 emission wavelengths. The fluorescence was measured with a spectrofluorimeter Cary Eclipse (Varian). $C_{12}E_8$ (1 mg/ml) and EGTA (4 mM) were added to obtain the maximum (due to the disruption of membranes) and minimum (due to the quelation of calcium) ratios of fluorescence, respectively. Calcium concentration was calculated as indicated in [33].

Measurement of mitochondrial membrane potential

To determine the mitochondrial membrane potential SHSY5Y cells were cultured in 35 mm dishes. After different TCDD treatments samples were washed twice with Tyrode's buffer containing 145 mM NaCl, 5 mM KCl, 10 mM glucose, 1.5 mM $CaCl_2$, 1 mM $MgCl_2$ and 10 mM HEPES pH 7.4. Then, cells were incubated with 20 nM tetramethyl rhodamine methyl ester (TMRM) (Sigma) in Tyrode's buffer during 45 min in darkness. After the incubation period, samples were visualized using fluorescence Axoplan Zeiss microscope with excitation and emission wavelengths of 549 and 573 nm, respectively. Fluorescence intensity was evaluated using the ImageJ software.

Propidium iodide (PI) hypodiploid apoptosis assay

TCDD was added at 250 nM concentration. Supernatant of treated SHSY5Y cells was collected and centrifuged 5 min at 600×*g*. 800 μl of Vindelov solution (0,01 mM TRIS, 10 mM NaCl, 0,1 mg/ml RNAase and 0.1 % Tween) was added to the plate and mixed gently by pipetting, observing the nucleus release under the microscope. The nucleus were added to the centrifugated supernatant and mixed gently by pipetting. Samples were centrifuged 8 min at 800×*g* and the pellet was resuspended in 500 μl of PBS and 0,003 % PI was added. To quantify the percentage of hypodiploid cells (sub-G1 phase), samples were processed and data acquired in a Cytomycs FC-500 flow cytometer (Beckman Coulter).

Sarcoplasmic reticulum vesicles preparation

Sarcoplasmic reticulum (SR) vesicles were prepared from rabbit fast-twitch skeletal muscle as previously described [21, 34]. Protein concentration was either determined by the method of Lowry using bovine serum albumin as standard, or deduced from absorption measurements at 280 nm in the presence of 1 % SDS, as in [35].

Fluorescence anisotropy measurements

Fluorescence probe trimethyl ammonium 1,6-diphenyl-1,3,5-hexatriene (TMA-DPH, Invitrogen) was used to test SR membrane fluidity in the absence and the presence of TCDD. Briefly, 30 ng/ml final probe concentration was added to 50 μg SR protein/ml in 2 ml of buffer containing 200 mM Mops-Tris pH 7.4, 2 mM EGTA and 5 mM $MgCl_2$, at 25 °C, in darkness with shaking for 15 min. Fluorescence intensity measurements were carried out at 25 °C with excitation and emission wavelengths of 360 and 430 nm, respectively, and polarization filters in the parallel and perpendicular orientations. The fluorescence was measured with a spectrofluorimeter Cary Eclipse (Varian). Fluorescence anisotropy was calculated as r value as described by the following equation:

$$r = (I_{VV} - G \times I_{VH})/(I_{VV} + 2 \times G \times I_{VH})$$

where I_{VV} and I_{VH} are the fluorescence intensities (H is horizontal and V is vertical orientation of the excitation and emission polarizer, respectively) and $G = I_{HV}/I_{HH}$ is the instrumental factor. Lower values of anisotropy correspond to greater membrane fluidity.

Statistical analysis of the data

Statistical analysis was carried out using one-way ANOVA tests followed by post hoc Tukey tests using Prism 5.0 software (GraphPad). Significance was set at $P < 0.05$. Data shown are mean ± SD.

Results

TCDD induces apoptosis in SHSY5Y cells

We first analyzed the cell death process (e.g. necrosis or apoptosis) that takes place after TCDD incubation of SHSY5Y human neuroblastoma cells. TCDD toxicity in SHSY5Y cells was evaluated in cultures incubated with dioxin using concentrations ranging from 10 nM to 1 μM for 90 min. Cell death was measured using the MTT reduction assay after 18–24 h of additional incubation in fresh complete medium without TCDD. This set of experiments allowed us to calculate an EC_{50} value of loss in viability induced by TCDD of 292 ± 28 nM (Fig. 1a). This value is similar to that calculated for NGF-differentiated PC12 cell line (218 ± 24 nM, [27]) and two times the value obtained using cerebellar granule cells (127 ± 21 nM, [28]). To validate the results of cell death obtained from MTT analysis, we also measured TCDD-induced cell death in SHSY5Y cultures using the trypan blue exclusion assay. The comparison between both

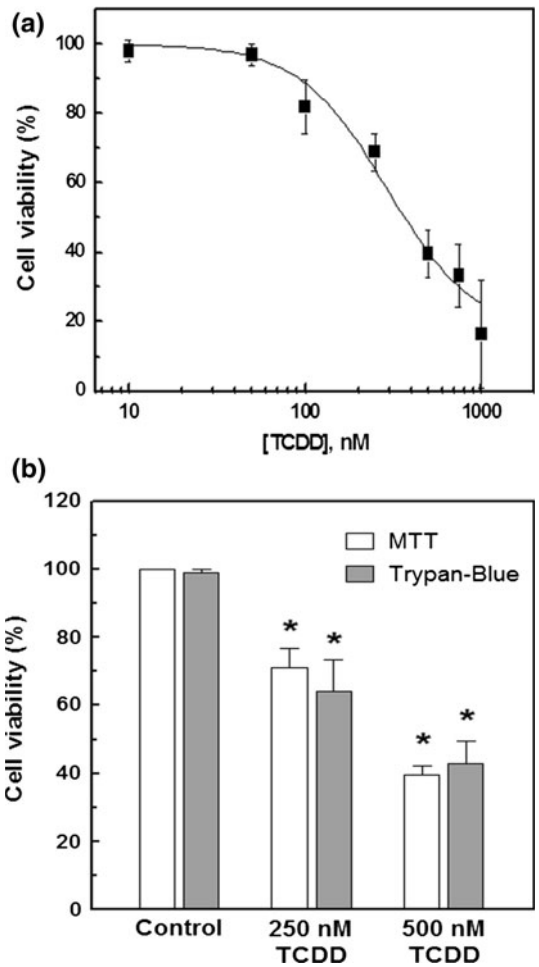

Fig. 1 Concentration dependence of TCDD toxicity in SHSY5Y human neuroblastoma cells. **a** SHSY5Y cells were incubated with different TCDD concentrations (10, 50, 100, 250, 500, 750 and 1,000 nM) for 90 min. Cell death was determined by the MTT reduction assay between 18 and 24 h after TCDD treatment. The EC_{50} value (292 ± 28 nM) was calculated using the logistic dose response curve from Origin™ software. **b** Comparison between MTT reduction and trypan exclusion assays in TCDD-induced cell death. SHSY5Y cells were incubated with 250 and 500 nM TCDD concentrations and cell death was assayed using both cell viability assays. Data shown are mean ± SD ($n \geq 6$). *$P < 0.05$ (different from control)

viability assays, MTT and trypan blue, was carried out at two different TCDD concentrations: 250 and 500 nM. The results obtained clearly indicated that the decrease of cell viability is similar in both cases 65–70 % and 40–45 %, respectively (Fig. 1b).

To discriminate between TCDD-induced apoptosis or necrosis in SHSY5Y cultures we measured caspase-3 activity that is widely considered a good marker of apoptotic cell death. Thus, Fig. 2a shows caspase-3 activity measurements following TCDD incubation of SHSY5Y cells. Incubation of SHSY5Y cultures with 250 nM TCDD (a concentration close to the EC_{50} value) for 90 min

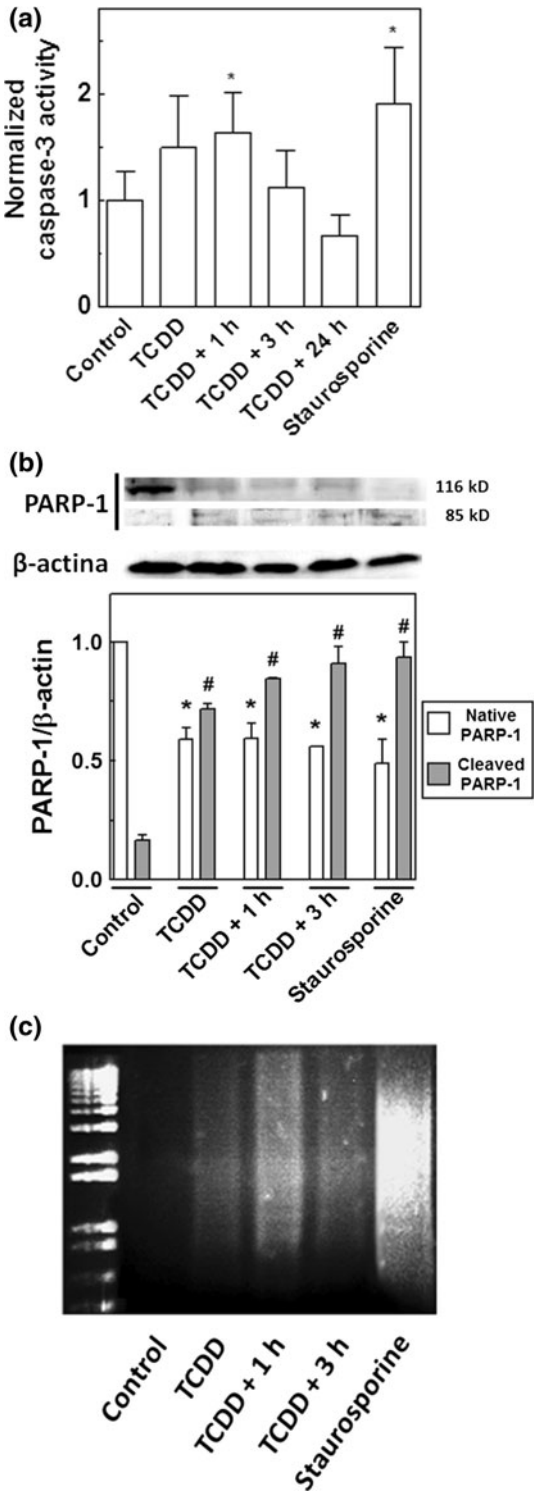

Fig. 2 TCDD induces apoptosis in SHSY5Y cells. SHSY5Y cells were treated with 250 nM TCDD for 90 min and apoptosis markers were analyzed after TCDD incubation and after 1, 3 and 24 h of additional incubation without TCDD. Staurosporine (24 h incubation time) was used as a positive control of apoptosis; (*, #) $P < 0.05$ (different from control). **a** TCDD increases caspase-3 activity. **b** Immunoblotting detection of native uncleaved (116 kDa) and cleaved (85 kDa) forms of PARP-1 in SHSY5Y cells. **c** TCDD induces nucleosomal DNA fragmentation (DNA laddering) in SHSY5Y cells

produced an increment of caspase-3 activity that reached the maximum (1.5–2-fold increase) at 1 h after TCDD treatment (Fig. 2a). The caspase-3 activity decreased to control levels 24 h after TCDD incubation. As a positive control, SHSY5Y cells were treated with 30 nM staurosporine [36]. The treatment with this apoptotic inducer for 24 h also provoked a twofold increase in caspase-3 activity (Fig. 2a).

To further describe about the apoptotic death induced by TCDD, we analyzed PARP-1 integrity which is a target of caspase-3 during apoptosis [37]. Incubation of SHSY5Y cultures with 250 nM TCDD for 90 min produced a decrease of intact PARP-1 and an appearance of cleaved form of PARP as revealed by western blot analysis, and this decrease/appearance is also observed at 1 and 3 h after TCDD treatment (Fig. 2b). Again, the treatment with staurosporine produced a similar pattern of PARP-1 fragmentation (Fig. 2b). As a consequence of caspases activation, a nuclear fragmentation takes place in the cell. This process can be analyzed as a DNA laddering using electrophoretic approaches. Using the same experimental conditions than in caspase-3 activity and PARP-1 fragmentation, after 250 nM TCDD treatment an extensive DNA laddering is observed in SHSY5Y cultures and it can be seen at 1 and 3 h after TCDD treatment (Fig. 2c). As expected, staurosporine generated a characteristic DNA laddering of an apoptotic process (Fig. 2c).

In addition, we studied the ploidy status of SHSY5Y cells in presence of 250 nM TCDD for 90 min by flow cytometry analysis using PI staining. We found that TCDD increases the area of the peak corresponding to hypodiploid, apoptotic DNA content (~30 %) as compared to control untreated cells (~5 %) (Fig. 3). The hypodiploid DNA content increases 1 and 3 h after TCDD treatment up to 35 % and 40–45 %, respectively, in a similar way to that found with staurosporine (40 %) as a positive control of apoptosis (Fig. 3).

Nuclear chromatin organization can be visualized by fluorescence microscopy using DNA-binding fluorescent dye DAPI. An apoptotic process shows a characteristic fragmented chromatin. To complete the analysis of the cell death process induced by TCDD in SHSY5Y cells, we have taken photographs using a fluorescence microscope under the different experimental conditions studied. In absence of TCDD, control cultures showed nuclei

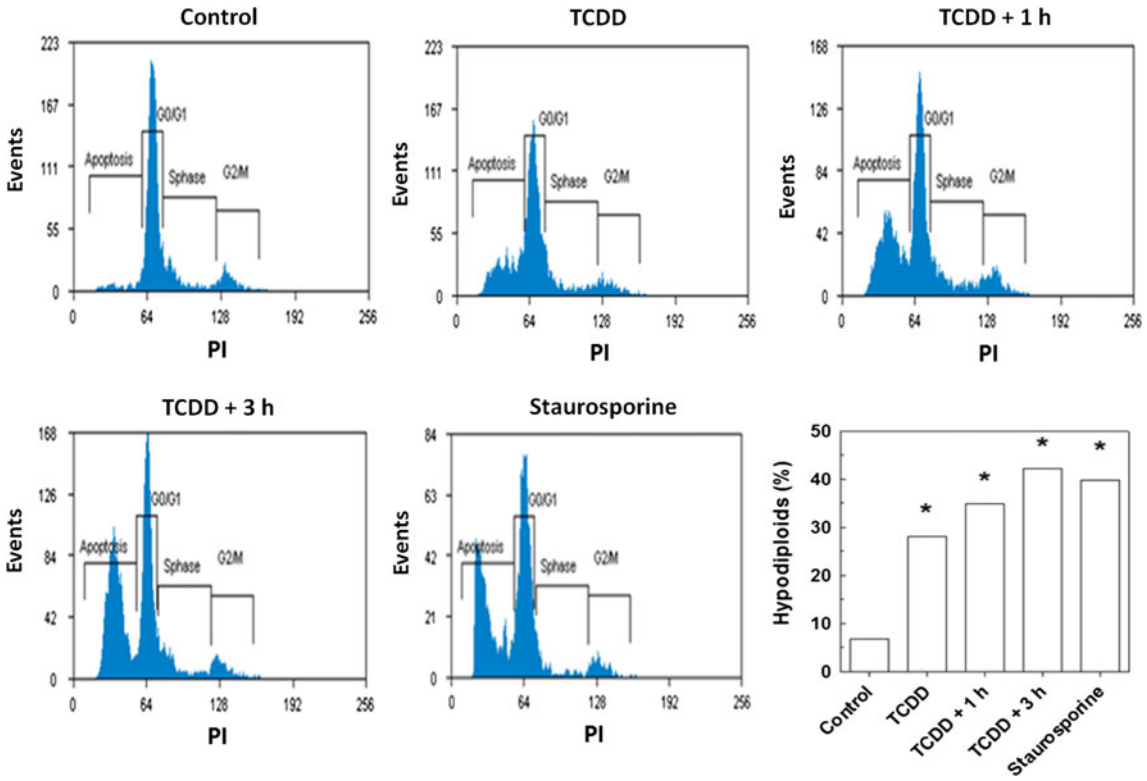

Fig. 3 TCDD increases the hypodiploid (apoptotic) DNA content in SHSY5Y cells. SHSY5Y cells were treated with 250 nM TCDD for 90 min and cell cycle phases distribution and hypodiploid DNA content were analyzed by flow cytometry (cell staining was made with PI) after TCDD incubation and after 1 and 3 h of additional incubation without TCDD. Cells without any treatment are indicated as control panel. Staurosporine (24 h incubation time) was used as a positive control of apoptosis. Quantification of hypodiploid content from all the conditions assayed is also shown in the additional panel

with low intensity DAPI labeling reflecting a homogeneous chromatin distribution (Fig. 4a, control). Chromatin condensation, denoted by an intense DAPI labeling, was observed after TCDD incubation at 250 nM concentration (Fig. 4a, TCDD). The typical pattern of nuclear fragmentation of apoptotic nuclei was observed 1, 3 and, particularly, 6 h after TCDD incubation (Fig. 4a). As a control, the incubation with staurosporine also provoked similar nuclear condensation to that observed with TCDD (Fig. 4a, staurosporine). We have performed the quantification of apoptotic cells (considered those showing nuclear fragmentation) under the different conditions assayed. The percentage of cells that have their nuclei fragmented increases from 2 to 3 % under control conditions, to around 30 % of the cells after TCDD treatment (Fig. 4b). This percentage of apoptotic cells observed from fluorescence images fits well to that obtained from the viability assays, approx. 30 % at 250 nM TCDD concentration (Fig 1). The quantification of SHSY5Y cells incubated in the presence of staurosporine retrieved a ~22 % of cells with fragmented nuclei (Fig. 4b). Altogether, these results allow us to conclude that TCDD toxicity takes place through an apoptotic process in SHSY5Y cells.

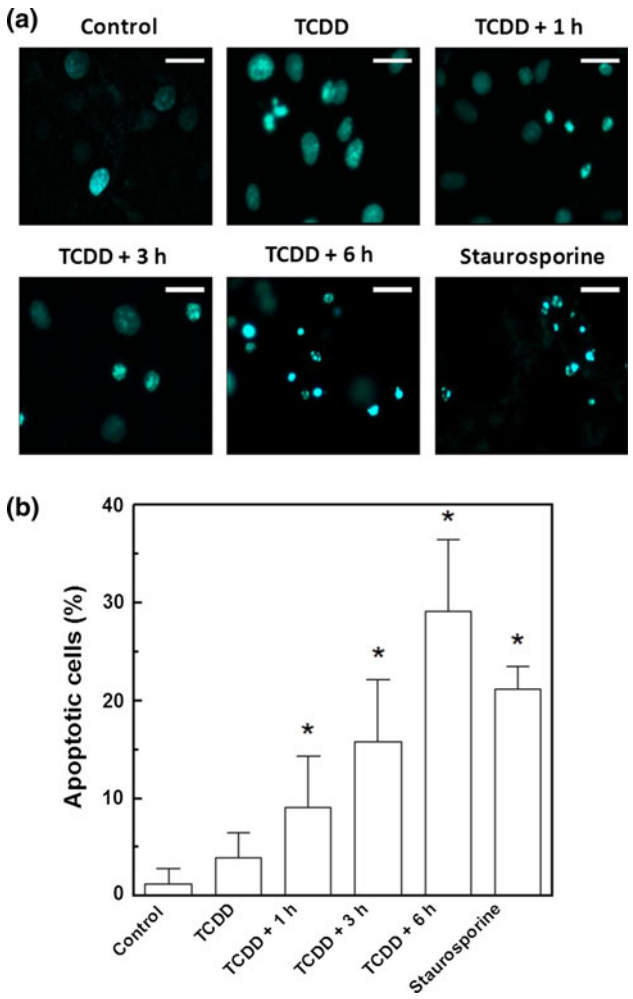

Fig. 4 TCDD induces nuclear fragmentation in SHSY5Y cells. **a** Chromatin condensation and nuclear fragmentation were analyzed by fluorescence microscopy using the DNA-binding fluorescent dye DAPI. SHSY5Y cells were treated with 250 nM TCDD for 90 min and DAPI labeling was photographed after TCDD incubation and after 1, 3, 6 and 24 h of additional incubation without TCDD. Staurosporine (24 h incubation time) was used as a positive control of nuclear fragmentation. *Scale bar* 20 μm. **b** Quantification of apoptotic cells calculated from images shown in panel a. Data shown are mean ± SD ($n \geq 6$) and at least 500 cells were counted per experimental condition. *$P < 0.05$ (different from control)

TCDD disrupts calcium homeostasis in SHSY5Y cells

Calcium homeostasis is critical to cell physiology and its perturbation can result in cell death [38]. Due to this, we analyzed at different times the cytoplasmic calcium concentration after TCDD treatment of SHSY5Y cells using the fluorescent dye Fluo 3-AM. Control cells, in the absence of TCDD, did not show Fluo-3 signal (Fig. 5a, control). This is consistent with a low micromolar cytoplasmic calcium concentration. Incubation with 250 nM TCDD (up to 90 min) resulted in an increase of Fluo-3 fluorescence, as a consequence of a cytoplasmatic calcium concentration increase, reaching the maximum at 60 min of TCDD treatment (Fig. 5a images, b quantification). This increase in cytoplasmic calcium concentration is sustained up to 3 h after the TCDD treatment, and the fluorescence starts to slightly decrease at 6 h after TCDD incubation (Fig. 5a images, b quantification). As a positive control of cytoplasmatic calcium disruption, SHSY5Y cells were incubated with 500 μM zinc for 30 min. Zinc readily increased Fluo-3 fluorescence (Fig. 5a Zn^{2+}, b open circle). To better understand the TCDD-induced changes in calcium concentration, we performed similar TCDD toxicity assays in PBS used as a calcium-free medium. TCDD toxicity assay up to 90 min in this medium produces increases of cytoplasmatic calcium concentration reaching the maximum at 30 min of dioxin incubation that is the 50 % observed with calcium-added medium (Fig. 6). After 90 min of TCDD treatment the cytoplasmic calcium concentration decreased to control values (Fig. 6). These results suggest that the stored calcium from intracellular deposits has a role in TCDD-dependent toxicity in SHSY5Y cells.

TCDD induces the loss of the mitochondrial membrane potential

It is well established that loss of mitochondrial membrane potential, as a consequence of calcium overload, can cause

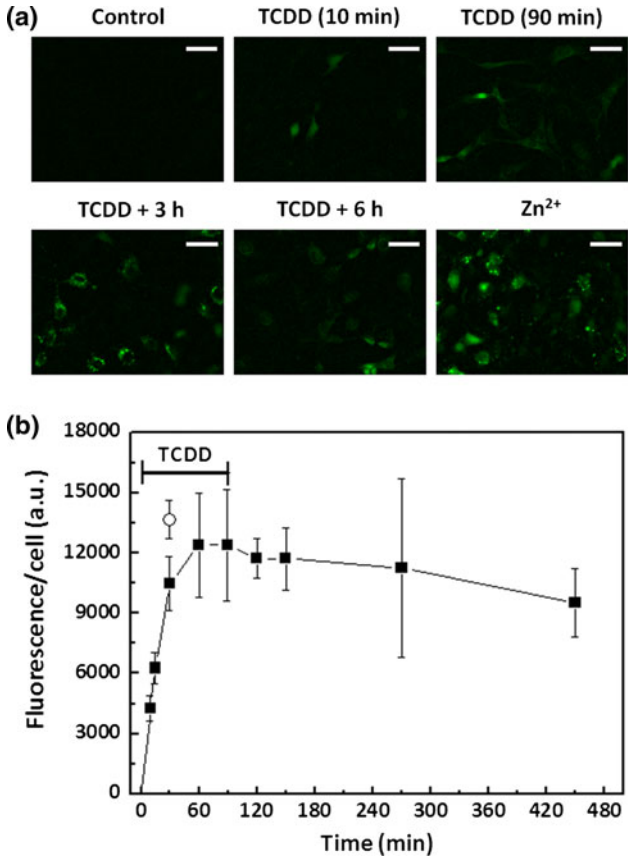

Fig. 5 TCDD increases the intracellular Ca^{2+} concentration in SHSY5Y cells. **a** SHSY5Y cells were treated with 250 nM TCDD. Images were taken from 10 to 90 min of incubation with TCDD and after 1–6 h of additional incubation after TCDD exposure. Zn^{2+} (at 500 μM, 30 min incubation time) was used as a positive control of cytosolic Ca^{2+} increase. *Scale bar* 20 μm. **b** Quantification of the fluorescence observed per cell. Data shown are mean ± SD ($n \geq 6$) and at least 500 cells were counted per experimental condition. TCDD (*closed squares*) and Zn^{2+} (*open circle*)

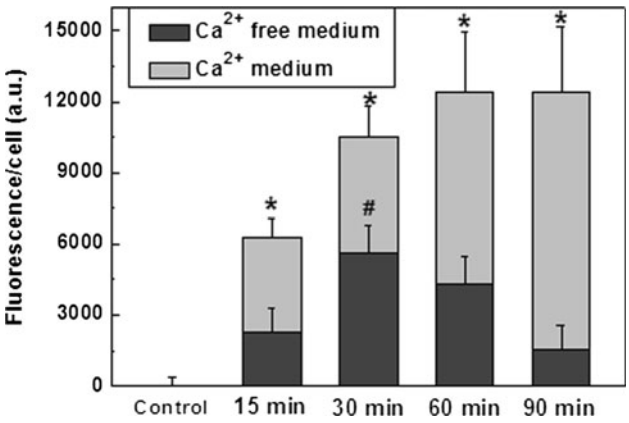

Fig. 6 Comparison of TCDD-induced intracellular calcium increase measured by Fluo-3 fluorescence in calcium-free medium (*black bars*) and calcium-added medium (*grey bars*). TCDD was used at 250 nM concentration at different times of incubation up to 90 min. Data shown are mean ± SD ($n \geq 6$). (*, #) $P < 0.05$ (different from control)

apoptosis [39]. Thus, we analyzed the mitochondrial membrane potential in SHSY5Y cells after TCDD treatments using the fluorescent dye TMRM. In the absence of TCDD, control SHSY5Y cells showed high intensity of TMRM labeling due to the localization of fluorescent dye in active mitochondria (Fig. 7a, control). Incubation of SHSY5Y cells with 250 nM TCDD for 90 min produced a decrease of TMRM fluorescence of approx. a 30–35 % reflecting a descent of mitochondrial membrane potential and, after a slightly recovery, is finally maintained at 6 and 24 h after TCDD treatment in a 25–30 % (Fig. 7a images, b closed squares). This result is consistent with the reduced cell viability, ~30 %, obtained with 250 nM TCDD concentration (Fig. 1). In agreement with these results, when the analysis of the mitochondrial membrane potential is carried out with 5 nM TCDD concentrations (cell death lower than 5 %), the same initial decrease in fluorescence can be observed during TCDD incubation, but a fully recovery is measured at 6 and 24 h after TCDD treatment (Fig. 7b, closed circles). Again, treatment with staurosporine for 24 h was used as a positive control of apoptosis, and a similar mitochondrial membrane potential reduction to that observed with 250 nM TCDD is measured (Fig. 7a images, b open circle). These results suggest that TCDD toxicity in SHSY5Y cells takes place through a loss of mitochondrial membrane potential.

TCDD induces changes in anisotropy and calcium leakage in SR membranes

The results shown above indicate that TCDD treatment causes an increment of intracellular calcium concentration coming from both the exterior of the cell and intracellular stores. This elevation induces or not cell death depending of the intensity of TCDD insult. Thus, we try to define the target of the dioxin in the cell. Due to the high lipophilic character of TCDD [19], we consider that cell membranes could be the main target of the dioxin. To analyze this hypothesis, we used a well-known membrane model: the SR vesicles prepared as described in Methods. First, we measured the calcium transport induced by TCDD in Ca^{2+}-loaded SR membranes by using the fluorescence probe Fura-2. Under control conditions, external calcium concentration is 6.1 ± 1.1 μM, a low micromolar concentration typically present in distilled water. The addition of 0.5 μM TCDD did not produce a change in external calcium concentration (6.1 ± 1.7 μM) but 1 and 3 μM TCDD-induced a significant increase up to 60.7 ± 7.6 and 88.7 ± 8.7 μM, respectively (Fig. 8a). These results suggest that TCDD produce a membrane leak that allows the empty of Ca^{2+}-loaded SR membranes. These suggested structural alterations of the membrane can be monitored

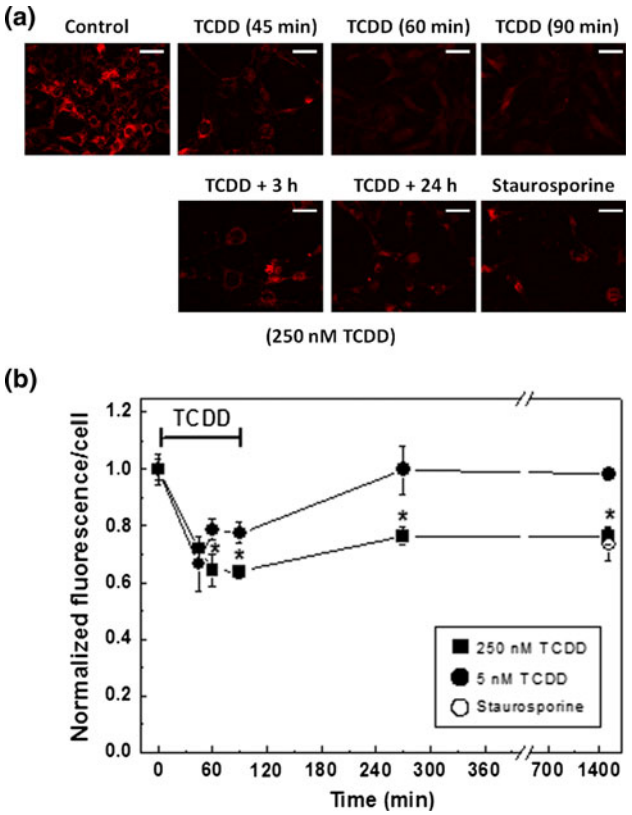

Fig. 7 TCDD effect on the mitochondrial membrane potential in SHSY5Y cells. **a** Mitochondrial membrane potential was analyzed by fluorescence microscopy using fluorescent dye TMRM after treatment of SHSY5Y cells with 250 nM TCDD at different times and after additional incubation without TCDD. *Scale bar* 20 μm. **b** Normalized TMRM fluorescence of SHSY5Y cells treated with 5 and 250 nM TCDD at different times. Data shown are mean ± SD ($n \geq 6$) and at least 500 cells were counted per experimental condition. TCDD (*closed squares*, *closed circles*) and staurosporine (*open circle*). (*)$P < 0.05$ (different from control)

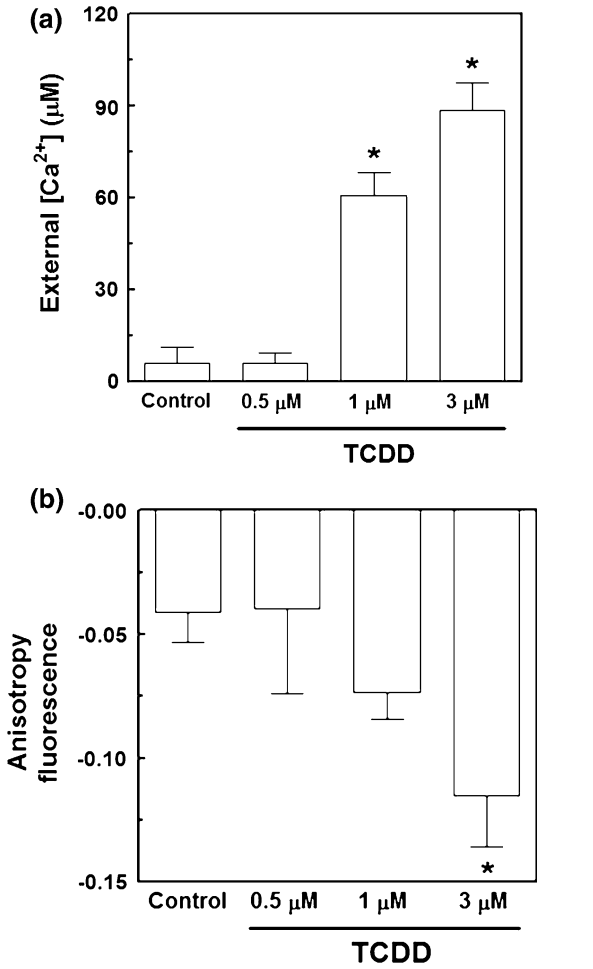

Fig. 8 TCDD produces structural alteration in membranes. **a** Ca^{2+} passive permeability TCDD-induced from Ca^{2+}-loaded sarcoplasmic reticulum (SR) vesicles. **b** Anisotropy fluorescence changes induced by TCDD in SR vesicles measured using the fluorescence of TMA-DPH. Anisotropy theoretically ranges from −0.2 to 0.4. *$P < 0.05$ (different from control)

with anisotropy measurements using the fluorescence probe TMA-DPH. The anisotropy was measured in a spectrofluorimeter equipped with polarizers, and the results are shown in Fig. 8b. The addition of TCDD to SR membranes produced a significant decrease of anisotropy that reflects an increase of the fluidity of the membrane. The decrease of anisotropy induced by TCDD (Fig. 8b) fits well with the calcium passive permeability produced by the dioxin (Fig. 8a) with similar effects at the TCDD concentrations assayed. An EC_{50} value for TCDD effects in SR membranes can be calculated from both set of experiments (0.9–1 μM TCDD).

Discussion

The dioxin (TCDD) is a highly toxic xenobiotic agent that is very persistent in the different organs of the body, included the brain [40]. In the last three decades, TCDD toxicity in the nervous system have been analyzed, focusing on its negative effects with developmental and behavioral analysis in animals and humans exposed to this dioxin during the gestational periods [6–11]. More recent studies have shown that fetal exposure of TCDD causes defects in the male reproductive system [41, 42] and alters myelination and gliogenic potential of the mature CNS of the rat [43]. Also, this dioxin disrupts neurogenesis of cerebellar granule cells in mouse [44]. Albeit the efforts have been intensified to determine the molecular mechanisms, the signaling pathways involved and the molecular targets in neurons of dioxin-induced neurotoxicity, these issues are still to be elucidated.

Several studies have been performed using primary neuronal cultures to explore the molecular level the TCDD toxicity. Interestingly, in cerebellar granular cells the dioxin produces the translocation of protein kinase C

(PKC) from cytosol to the plasma membrane through the receptor for activated C kinase (RACK-1) [45]. In addition, different studies performed in cortical neurons have implicated glutamate receptors of the *N*-methyl-D-aspartate (NMDA) subtype in TCDD toxicity by increasing intracellular calcium concentration [16, 18], which was linked with AhR-mediated gene expression [17, 18].

Previous studies from our group showed that TCDD induces cell death through an apoptotic process in both NGF-differentiated PC12 and cerebellar granule cells cultures but with different contribution of AhR in this process. While in NGF-differentiated PC12 cells the role of AhR in TCDD toxicity was not prominent [27], in cerebellar granule cells this receptor was clearly involved in TCDD toxicity [28]. As TCDD acts like a tumor promoter in different cell types by inhibition of apoptosis [46], the induction of apoptosis is a controversial issue which it has been showed in other cells like thymocytes [47, 48]. In the particular case of SHSY5Y cells we have found low AhR expression and the assayed blockers of this receptor, resveratrol and α-naphthoflavone, induced a high level of cell death (data not shown). Thus, we could not test the actual role of this receptor in TCDD-induced apoptosis.

Our results show that TCDD toxicity cause loss of viability in SHSY5Y with an EC_{50} value of 292 ± 28 nM, in the same order of magnitude to those obtained in NGF-differentiated PC12 cells and cerebellar granule cells [27, 28]. TCDD toxicity in SHSY5Y cells involves an apoptotic process. This fact is supported by increased caspase-3 activity, PARP-1 fragmentation, DNA laddering, hypodiploid DNA content and nuclear fragmentation approaches. Moreover, staurosporine, the prototypical molecule of apoptosis induction [36] produces similar effects to that produced by TCDD. Altogether, these data display that SHSY5Y cells undergo apoptosis after TCDD treatment.

There are evidences showing that an excessive and sustained increment of cytosolic calcium concentration can produce cell death through an apoptotic pathway [49, 50]. TCDD neurotoxicity has been linked recently with the highly permeable to calcium NMDA-subtype of glutamate receptors [16–18]. In this work, we showed that TCDD causes an increase of cytosolic calcium concentration both in calcium-free and calcium-added medium, involving not only the extracellular calcium but the calcium from the intracellular stores. The set of experiments with the calcium-free medium indicates that intracellular calcium concentration partially returns to basal levels after the TCDD treatment, showing that the cation is buffered by the organelles of the cells or is eliminated by its extrusion out of the cell. These results could suggest that TCDD produces an increment of cytosolic calcium concentration coming from the endoplasmic reticulum and this increase produces a capacitative calcium entry coming from the exterior of the cell. Although this mechanism has been described for other drugs in neuronal cultures in vitro [51], and calcium release form the endoplasmic reticulum and capacitative calcium entry have been proposed to be apoptogenic [52], additional experiments have to be done to confirm this hypothesis. Also, the disruption of calcium homeostasis has been found to trigger apoptosis through loss of mitochondrial integrity and mitochondrial membrane potential [53, 54]. In agreement with this, the results presented in Figs. 5 and 7 indicated that the time course of intracellular calcium concentration increase fits well with the time course of mitochondrial membrane potential decrease. Mitochondrial membrane potential has been analyzed in different cell types after TCDD exposure and the dioxin produced both hyperpolarization [55, 56] and depolarization [57, 58]. These contradictory results could be due to a cell type specific problem. Our results are more consistent as we demonstrate that TCDD causes in SHSY5Y cells a decrease in mitochondrial membrane potential which is comparable in percentage with the loss of cell viability in culture.

The assessment of the TCDD targets in the cell is a crucial point. To develop protective treatments to avoid TCDD toxicity or, at least, ameliorate the dioxin effects in the human body, it is of great importance the definition of its molecular targets. The high lipophilic character of TCDD molecule suggests that cell membranes could constitute one of the main targets for the dioxin. We test this possibility by measuring passive Ca^{2+} efflux through a membrane model, SR vesicles, widely used to study active transport mediated by Ca^{2+}-ATPases. Data from this paper show passive calcium efflux induced by TCDD in the absence of ATP, suggesting that the cation transport takes place through the membrane probably by transient pores formed by the dioxin. If that possibility is correct, the anisotropy of the membrane had to be affected, as this fluorescence parameter reflects the structural organization of the membrane as a measure of its fluidity. Our data are clear showing a decrease of the anisotropy close to three-times that indicates a marked increase in membrane fluidity. In a good agreement with our results, changes in anisotropy induced by TCDD have been previously described [55, 59]. The EC_{50} value obtained in this set of experiments is 0.9–1 μM TCDD that is three-times the EC_{50} value of TCDD toxicity in SHSY5Y cells (0.29 μM), but it has to be taken into account that we are using two different model of membranes.

In summary, the results presented in this paper showed that TCDD-induced cell death in SHSY5Y human neuroblastoma cells takes place through an apoptotic process, that is initiated by a calcium homeostasis disruption that lead to a loss of mitochondrial membrane potential. The cell membranes are targets for TCDD that produce

membrane structural alterations underlying the calcium homeostasis disruption. Taken together, these findings suggest that the disruption in calcium homeostasis plays an important role in TCDD-induced neurotoxicity. Future work will be conducted to unravel the molecular mechanisms of TCDD neurotoxicity using membrane models to determine the TCDD effects on membrane integrity.

Acknowledgments This study was supported by a Grant from the Junta de Extremadura, Spain (PRI07A019 to JM Merino), Junta de Extremadura (GRU10008) and from the Red Temática de Investigación Cooperativa en Cáncer (RTICC) (RD 06/020/1016, Fondo de Investigaciones Sanitarias (FIS), Carlos III Institute, Spanish Ministry of Health). AM-H, FJS-M and MPH-V are the recipients of predoctoral fellowships from the Junta de Extremadura (Spain). All Spanish funding is co-sponsored by the European Union FEDER program.

Conflict of interests None.

References

1. Ahmed RG (2011) Perinatal TCDD exposure alters developmental neuroendocrine system. Food Chem Toxicol 49:1276–1284
2. Mates JM, Segura JA, Alonso FJ, Marquez J (2010) Roles of dioxins and heavy metals in cancer and neurological diseases using ROS-mediated mechanisms. Free Rad Biol Med 49: 1328–1341
3. Shibamoto T, Yasuhara A, Katami T (2007) Dioxin formation from waste incineration. Rev Environ Contam Toxicol 190:1–41
4. Bock KW, Kohle C (2006) Ah receptor: dioxin-mediated toxic responses as hints to deregulated physiologic functions. Biochem Pharmacol 72:393–404
5. Mimura J, Fujii-Kuriyama Y (2003) Functional role of AhR in the expression of toxic effects by TCDD. Biochim Biophys Acta 1619:263–268
6. Schantz SL, Ferguson SA, Bowman RE (1992) Effects of 2,3,7, 8-tetrachlorodibenzo-*p*-dioxin on behavior of monkeys in peer groups. Neurotoxicol Teratol 14:433–446
7. Schantz SL, Bowman RE (1989) Learning in monkeys exposed perinatally to 2,3,7,8-tetrachlorodibenzo-*p*-dioxin (TCDD). Neurotoxicol Teratol 11:13–19
8. Rogan WJ, Gladen BC (1992) Neurotoxicology of PCBs and related compounds. Neurotoxicology 13:27–35
9. Jacobson JL, Jacobson SW (1996) Intellectual impairment in children exposed to polychlorinated biphenyls in utero. N Engl J Med 335:783–789
10. Jacobson JL, Jacobson SW (1997) Evidence for PCBs as neurodevelopmental toxicants in humans. Neurotoxicology 18:415–424
11. Jacobson JL, Jacobson SW (1997) Teratogen update: polychlorinated biphenyls. Teratology 55:338–347
12. Legare ME, Hanneman WH, Barhoumi R, Burghardt RC, Tiffany-Castiglioni E (2000) 2,3,7,8-Tetrachlorodibenzo-*p*-dioxin alters hippocampal astroglia-neuronal gap junctional communication. Neurotoxicology 21:1109–1116
13. Nayyar T, Zawia NH, Hood DB (2002) Transplacental effects of 2,3,7,8-tetrachlorodibenzo-*p*-dioxin on the temporal modulation of Sp1 DNA binding in the developing cerebral cortex and cerebellum. Exp Toxicol Pathol 53:461–468
14. Collins LL, Williamson MA, Thompson BD, Dever DP, Gasiewicz TA, Opanashuk LA (2008) 2,3,7,8-Tetracholorodibenzo-*p*-dioxin exposure disrupts granule neuron precursor maturation in the developing mouse cerebellum. Toxicol Sci 103:125–136
15. Boas M, Feldt-Rasmussen U, Main KM (2012) Thyroid effects of endocrine disrupting chemicals. Mol Cell Endocrinol 355:240–248
16. Kim SY, Yang JH (2005) Neurotoxic effects of 2,3,7,8-tetrachlorodibenzo-*p*-dioxin in cerebellar granule cells. Exp Mol Med 37:58–64
17. Lin CH, Chen CC, Chou CM, Wang CY, Hung CC, Chen JY, Chang HW, Chen YC, Yeh GC, Lee YH (2009) Knockdown of the aryl hydrocarbon receptor attenuates excitotoxicity and enhances NMDA-induced BDNF expression in cortical neurons. J Neurochem 111:777–789
18. Lin CH, Juan SH, Wang CY, Sun YY, Chou CM, Chang SF, Hu SY, Lee WS, Lee YH (2008) Neuronal activity enhances aryl hydrocarbon receptor-mediated gene expression and dioxin neurotoxicity in cortical neurons. J Neurochem 104:1415–1429
19. Marinkovic N, Pasalic D, Ferencak G, Grskovic B, Stavljenic Rukavina A (2010) Dioxins and human toxicity. Arh Hig Rada Toksikol 61:445–453
20. Hu W, Jones PD, DeCoen W, King L, Fraker P, Newsted J, Giesy JP (2003) Alterations in cell membrane properties caused by perfluorinated compounds. Comp Biochem Physiol C 135:77–88
21. Hortigon-Vinagre MP, Chardonnet S, Montigny C, Gutierrez-Martin Y, Champeil P, Henao F (2011) Inhibition by 4-hydroxynonenal (HNE) of Ca^{2+} transport by SERCA1a: low concentrations of HNE open protein-mediated leaks in the membrane. Free Rad Biol Med 50:323–336
22. Zundorf G, Reiser G (2011) Calcium dysregulation and homeostasis of neural calcium in the molecular mechanisms of neurodegenerative diseases provide multiple targets for neuroprotection. Antioxid Redox Signal 14:1275–1288
23. Biedler JL, Helson L, Spengler BA (1973) Morphology and growth, tumorigenicity, and cytogenetics of human neuroblastoma cells in continuous culture. Cancer Res 33:2643–2652
24. Busciglio J, Yankner BA (1995) Apoptosis and increased generation of reactive oxygen species in Down's syndrome neurons in vitro. Nature 378:776–779
25. Sanfeliu C, Cristofol R, Toran N, Rodriguez-Farre E, Kim SU (1999) Use of human central nervous system cell cultures in neurotoxicity testing. Toxicol In Vitro 13:753–759
26. Chopra M, Schrenk D (2011) Dioxin toxicity, aryl hydrocarbon receptor signaling, and apoptosis-persistent pollutants affect programmed cell death. Crit Rev Toxicol 41:292–320
27. Sanchez-Martin FJ, Fernandez-Salguero PM, Merino JM (2010) 2,3,7,8-Tetrachlorodibenzo-*p*-dioxin induces apoptosis in neural growth factor (NGF)-differentiated pheochromocytoma PC12 cells. Neurotoxicol 31:267–276
28. Sanchez-Martin FJ, Fernandez-Salguero PM, Merino JM (2011) Aryl hydrocarbon receptor-dependent induction of apoptosis by 2,3,7,8-tetrachlorodibenzo-*p*-dioxin in cerebellar granule cells from mouse. J Neurochem 118:153–162
29. Mulero-Navarro S, Santiago-Josefat B, Pozo-Guisado E, Merino JM, Fernandez-Salguero PM (2003) Down-regulation of CYP1A2 induction during the maturation of mouse cerebellar granule cells in culture: role of nitric oxide accumulation. Eur J Neurosci 18: 2265–2272
30. Valera E, Sanchez-Martin FJ, Ferrer-Montiel AV, Messeguer A, Merino JM (2008) NMDA-induced neuroprotection in hippocampal neurons is mediated through the protein kinase A and CREB (cAMP-response element-binding protein) pathway. Neurochem Int 53:148–154
31. Sanchez-Martin FJ, Valera E, Casimiro I, Merino JM (2010) Nerve growth factor increases the sensitivity to zinc toxicity and

induces cell cycle arrest in PC12 cells. Brain Res Bull 81:458–466
32. Martin-Romero FJ, Garcia-Martin E, Gutierrez-Merino C (2002) Inhibition of oxidative stress produced by plasma membrane NADH oxidase delays low-potassium-induced apoptosis of cerebellar granule cells. J Neurochem 82:705–715
33. Grynkiewicz G, Poenie M, Tsien RY (1985) A new generation of Ca^{2+} indicators with greatly improved fluorescence properties. J Biol Chem 260:3440–3450
34. MacLennan DH (1970) Purification and properties of an adenosine triphosphatase from sarcoplasmic reticulum. J Biol Chem 245:4508–4518
35. De Foresta B, Henao F, Champeil P (1992) Kinetic characterization of the perturbation by dodecylmaltoside of sarcoplasmic reticulum Ca^{2+}-ATPase. Eur J Biochem 209:1023–1034
36. Weil M, Jacobson MD, Coles HS, Davies TJ, Gardner RL, Raff KD, Raff MC (1996) Constitutive expression of the machinery for programmed cell death. J Cell Biol 133:1053–1059
37. Kaufmann SH, Desnoyers S, Ottaviano Y, Davidson NE, Poirier GG (1993) Specific proteolytic cleavage of poly(ADP-ribose) polymerase: an early marker of chemotherapy-induced apoptosis. Cancer Res 53:3976–3985
38. Orrenius S, Zhivotovsky B, Nicotera P (2003) Regulation of cell death: the calcium-apoptosis link. Nat Rev Mol Cell Biol 4:552–565
39. Kroemer G, Galluzzi L, Brenner C (2007) Mitochondrial membrane permeabilization in cell death. Physiol Rev 87:99–163
40. Pohjanvirta R, Vartiainen T, Uusi-Rauva A, Monkkonen J, Tuomisto J (1990) Tissue distribution, metabolism, and excretion of ^{14}C-TCDD in a TCDD-susceptible and a TCDD-resistant rat strain. Pharmacol Toxicol 66:93–100
41. Bell DR, Clode S, Fan MQ, Fernandes A, Foster PM, Jiang T, Loizou G, MacNicoll A, Miller BG, Rose M, Tran L, White S (2007) Toxicity of 2,3,7,8-tetrachlorodibenzo-*p*-dioxin in the developing male Wistar (Han) rat. I: no decrease in epididymal sperm count after a single acute dose. Toxicol Sci 99:214–223
42. Bell DR, Clode S, Fan MQ, Fernandes A, Foster PM, Jiang T, Loizou G, MacNicoll A, Miller BG, Rose M, Tran L, White S (2007) Toxicity of 2,3,7,8-tetrachlorodibenzo-*p*-dioxin in the developing male Wistar(Han) rat. II: chronic dosing causes developmental delay. Toxicol Sci 99:224–233
43. Fernandez M, Paradisi M, D'Intino G, Del Vecchio G, Sivilia S, Giardino L, Calza L (2010) A single prenatal exposure to the endocrine disruptor 2,3,7,8-tetrachlorodibenzo-*p*-dioxin alters developmental myelination and remyelination potential in the rat brain. J Neurochem 115:897–909
44. Williamson MA, Gasiewicz TA, Opanashuk LA (2005) Aryl hydrocarbon receptor expression and activity in cerebellar granule neuroblasts: implications for development and dioxin neurotoxicity. Toxicol Sci 83:340–348
45. Lee HG, Kim SY, Choi EJ, Park KY, Yang JH (2007) Translocation of PKC-βII is mediated via RACK-1 in the neuronal cells following dioxin exposure. Neurotoxicol 28:408–414
46. Schwarz M, Buchmann A, Stinchcombe S, Kalkuhl A, Bock K (2000) Ah receptor ligands and tumor promotion: survival of neoplastic cells. Toxicol Lett 112–3:69–77
47. McConkey DJ, Hartzell P, Duddy SK, Hakansson H, Orrenius S (1988) 2,3,7,8-Tetrachlorodibenzo-*p*-dioxin kills immature thymocytes by Ca^{2+}-mediated endonuclease activation. Science 242:256–259
48. Kurl RN, Abraham M, Olnes MJ (1993) Early effects of 2,3,7,8-tetrachlorodibenzo-*p*-dioxin (TCDD) on rat thymocytes in vitro. Toxicology 77:103–114
49. Tombal B, Denmeade SR, Isaacs JT (1999) Assessment and validation of a microinjection method for kinetic analysis of $[Ca^{2+}]_i$ in individual cells undergoing apoptosis. Cell Calcium 25:19–28
50. Lynch K, Fernandez G, Pappalardo A, Peluso JJ (2000) Basic fibroblast growth factor inhibits apoptosis of spontaneously immortalized granulosa cells by regulating intracellular free calcium levels through a protein kinase Cdelta-dependent pathway. Endocrinology 141:4209–4217
51. Dow GS, Hudson TH, Vahey M, Koenig ML (2003) The acute neurotoxicity of mefloquine may be mediated through a disruption of calcium homeostasis and ER function in vitro. Malar J 2:14
52. Pinton P, Rizzuto R (2006) Bcl-2 and Ca^{2+} homeostasis in the endoplasmic reticulum. Cell Death Differ 13:1409–1418
53. Korge P, Weiss JN (1999) Thapsigargin directly induces the mitochondrial permeability transition. Eur J Biochem 265:273–280
54. Akao Y, Maruyama W, Shimizu S, Yi H, Nakagawa Y, Shamoto-Nagai M, Youdim MB, Tsujimoto Y, Naoi M (2002) Mitochondrial permeability transition mediates apoptosis induced by *N*-methyl(R)salsolinol, an endogenous neurotoxin, and is inhibited by Bcl-2 and rasagiline, *N*-propargyl-1(R)-aminoindan. J Neurochem 82:913–923
55. Shertzer HG, Genter MB, Shen D, Nebert DW, Chen Y, Dalton TP (2006) TCDD decreases ATP levels and increases reactive oxygen production through changes in mitochondrial F(0)F(1)-ATP synthase and ubiquinone. Toxicol Appl Pharmacol 217: 363–374
56. Tappenden DM, Lynn SG, Crawford RB, Lee K, Vengellur A, Kaminski NE, Thomas RS, LaPres JJ (2011) The aryl hydrocarbon receptor interacts with ATP5α1, a subunit of the ATP synthase complex, and modulates mitochondrial function. Toxicol Appl Pharmacol 254:299–310
57. Paajarvi G, Viluksela M, Pohjanvirta R, Stenius U, Hogberg J (2005) TCDD activates Mdm2 and attenuates the p53 response to DNA damaging agents. Carcinogenesis 26:201–208
58. Aly HA, Domenech O (2009) Cytotoxicity and mitochondrial dysfunction of 2,3,7,8-tetrachlorodibenzo-*p*-dioxin (TCDD) in isolated rat hepatocytes. Toxicol Lett 191:79–87
59. Alsharif NZ, Grandjean CJ, Murray WJ, Stohs SJ (1990) 2,3,7,8-Tetrachlorodibenzo-*p*-dioxin (TCDD)-induced decrease in the fluidity of rat liver membranes. Xenobiotica 20:979–988